PROCEEDINGS OF SCIENCE

Measurements of Transverse Spin Dependent $\pi^+\pi^-$ Azimuthal Correlation Asymmetry and Unpolarized $\pi^+\pi^-$ Cross-Section in pp Collisions at STAR

Babu Pokhrel, for the STAR Collaboration[a,*]

[a] *Temple University,*
1925 N 12th St, Philadelphia, US

E-mail: babu.pokhrel@temple.edu

The transversity distribution function, $h_1^q(x)$, encapsulates the transverse spin structure of the proton at the leading twist, where x represents the longitudinal momentum fraction carried by the quark q. The extraction of $h_1^q(x)$ poses a formidable challenge due to its chiral-odd nature. Measurements of final-state di-hadron pairs in transversely polarized proton-proton ($p^\uparrow p$) collisions directly probe the collinear quark transversity via coupling with a chiral-odd interference fragmentation function, IFF. This coupling results in an experimentally measurable azimuthal correlation asymmetry, A_{UT}. The asymmetry originates from the interplay between the spin orientation of the fragmenting quark and the resulting di-hadron in the final state. Thus, precise knowledge of unpolarized di-hadron fragmentation functions (FFs) is necessary to achieve a model-independent extraction of the transversity from these measurements. These FFs can be constrained by measuring the unpolarized di-hadron cross-section in pp collisions. We report the preliminary results on the A_{UT} for $\pi^+\pi^-$ pairs using $p^\uparrow p$ data collected by the STAR experiment at a center-of-mass energy ($\sqrt{s}$) of 200 GeV in 2015. Additionally, we report preliminary results of the unpolarized $\pi^+\pi^-$ cross section using pp data at $\sqrt{s}$ = 200 GeV collected in 2012. These datasets probe the valance quark region ($0.1 < x < 0.3$) at Q^2 of the order of $\sim$ 100 GeV^2.

25th International Spin Physics Symposium (SPIN 2023)
24-29 September 2023
Durham, NC, USA

[*] Speaker

1. Introduction

At the leading twist, the spin structure of the nucleon can be described by the three collinear parton distribution functions (PDFs): unpolarized PDF ($f_1(x)$), helicity PDF ($g_1(x)$), and transversity PDF ($h_1^q(x)$), where x is the fractional momentum of nucleon carried by the parton. While $f_1(x)$ and $g_1(x)$ are reasonably well-constrained by the global data [1, 2], our understanding of the $h_1^q(x)$ [3–6], is limited to measurements obtained from semi-inclusive deep inelastic scattering (SIDIS) experiments [7–12], e^+e^- collisions [13, 14], and $p^\uparrow p$ interactions [15, 16]. This limitation arises because $h_1^q(x)$ is a chiral-odd object, requiring coupling with another chiral-odd partner to form a chiral-even observable.

Transversity can be accessed through single-hadron production, such as Collins effect [17] in SIDIS or collinear factorization in hadronic collisions [18, 19]. Alternatively, transversity appears coupled with the interference fragmentation function (IFF) in unpolarized di-hadron production in hadronic collisions at leading twist [20–23]. This approach allows for the study of transversity without the need for jet reconstruction, eliminating associated systematic uncertainties and preserving collinear factorization.

The unpolarized di-hadron production channel in polarized proton-proton collisions ($p^\uparrow p$) provides convenient access to transversity coupled with the IFF. This coupling gives rise to an experimentally measurable azimuthal correlation asymmetry, denoted as A_{UT}, which originates from the interplay between the spin of the polarized quark and the final state di-hadron. However, isolating $h_1^q(x)$ from the A_{UT} requires experimental constraints on the IFF and unpolarized FF, $D_1^{h_1h_2}$, especially for gluons. Consequently, the global extraction of transversity relies on simulations, introducing substantial model-dependent uncertainties. The unpolarized di-hadron cross-section ($d\sigma_{UU}^{h_1h_2}$) in pp collisions offers a means to access $D_1^{h_1h_2}$, crucial for constraining transversity.

STAR initially observed a significant A_{UT} for $\pi^+\pi^-$ based on 2006 $p^\uparrow p$ data at a center-of-mass energy ($\sqrt{s}$) of 200 GeV [15]. Subsequently, further insights were gained by analyzing the 2011 dataset at $\sqrt{s} = 500$ GeV [16]. These measurements served as a proof-of-principle in $p^\uparrow p$, although the statistical uncertainties were substantial due to limited available statistics. This article reports preliminary results on the precision of the A_{UT} measurement based on 2015 $p^\uparrow p$ data and the $d\sigma_{UU}^{h_1h_2}$ results from 2012 pp data for $\pi^+\pi^-$ at $\sqrt{s} = 200$ GeV.

2. STAR Experiment and Datasets

The Relativistic Heavy-Ion Collider (RHIC) at Brookhaven National Laboratory can collide bunched beams of polarized protons up to $\sqrt{s} = 510$ GeV. The Solenoidal Tracker At RHIC (STAR) [24] is one of the major experiments, where the Time Projection Chamber (TPC) [25] is the core detector that provides particle tracking and particle identification (PID) in the mid-pseudorapidity region ($-1 < \eta < 1$) and over the whole 2π range in azimuthal angle. The time-of-flight detector (TOF) [26], with similar coverage as the TPC, improves the STAR's PID capability. The barrel electromagnetic calorimeter [27] provides event triggering based on the transverse energy (E_T) depositions in its towers cluster.

At RHIC, both beams exhibit stable polarization in the transverse direction to the collider plane. The polarization direction alternates in subsequent bunches, and the polarization pattern is modified from fill to fill to minimize systematic uncertainty. Although both beams maintain transverse polarization, integrating over all polarization states allows each beam to be treated as unpolarized, effectively reducing the net beam polarization to nearly zero. This enables measurements that require either or both beams to be unpolarized, such as single-spin asymmetry and unpolarized cross-section. The term "unpolarized cross-section" refers to the measurement from the unpolarized beams, and the "di-hadron" refers to the unpolarized $\pi^+\pi^-$ in the final state hereafter.

This measurement utilizes datasets collected by the STAR experiment at $\sqrt{s}$ = 200 GeV from the years 2012 and 2015. The 2015 dataset is employed for the IFF asymmetry measurement and features an integrated luminosity ($\mathcal{L}_{int}$) of 52 pb^{-1}. The selected physics events are triggered by jet-patch (JP) triggers JP1 and JP2 with E_T thresholds of 5.4 and 7.3 GeV, respectively. The 2012 dataset, a relatively smaller data sample corresponding to $\mathcal{L}_{int}$ = 14 pb^{-1}, is utilized for the unpolarized cross-section measurement for the $\pi^+\pi^-$. This dataset includes additional JP-triggered events, JP0, with a E_T = 3.5 GeV threshold. Including all three JP-triggered events, this dataset provides better gluon sensitivity, making it the optimal choice for the cross-section measurement.

Simulated events are required to estimate various systematic uncertainties and correct the detector effects in these measurements. For particle-level collision events, the PYTHIA 6 Monte Carlo event generator [28] is employed, utilizing the Perugia 12 tune [29] with a modified parameter (PARP(90)=0.213) [30]. This setup incorporates the CTEQ6 PDF sets [31]. Subsequently, the STAR detector response to the PYTHIA events is simulated using GEANT3 [32], considering the corresponding STAR detector configurations. Before reconstruction, the raw simulated detector responses are combined event-by-event with actual detector responses from the zero bias trigger samples, which represent random detector states, to simulate the beam backgrounds (embedding process). The produced simulation sample provides a very good description of the datasets.

3. $\pi^+\pi^-$ Azimuthal Correlation Asymmetry

3.1 Analysis

The A_{UT} for the $\pi^+\pi^-$ pairs is extracted using the cross-ratio formula [33],

$$A_{UT} \cdot \sin(\phi_{RS}) = \frac{1}{P} \cdot \frac{\sqrt{N^{\uparrow}(\phi_{RS})N^{\downarrow}(\phi_{RS}+\pi)} - \sqrt{N^{\downarrow}(\phi_{RS})N^{\uparrow}(\phi_{RS}+\pi)}}{\sqrt{N^{\uparrow}(\phi_{RS})N^{\downarrow}(\phi_{RS}+\pi)} + \sqrt{N^{\downarrow}(\phi_{RS})N^{\uparrow}(\phi_{RS}+\pi)}} \tag{1}$$

where, $N^{\uparrow(\downarrow)}$ is the number of $\pi^+\pi^-$ pairs, when the beam polarization is up(down). P is the average beam polarization, which is $\sim$ 57% for a beam traveling clockwise (blue) and $\sim$ 58% for the beam traveling counterclockwise (yellow). The definition of azimuthal angle $\phi_{RS}(= \phi_S - \phi_R)$ is illustrated in Fig. 1 [15], where ϕ_S is an angle between the polarization vector, $\vec{S}_a$, and the scattering plane, formed by the beam momentum vector, $\vec{p}_{beam}$, and the di-hadron momentum sum vector, $\vec{p}_h(= \vec{p}_{h,1} + \vec{p}_{h,2})$. ϕ_R is an angle between the scattering plane and the di-hadron plane, formed by two hadrons' momenta, $\vec{p}_{h,1}$, and $\vec{p}_{h,2}$. $\vec{R}(= \frac{1}{2}(\vec{p}_{h,1} - \vec{p}_{h,2}))$ is the relative momentum vector of the di-hadron system. Here, $\vec{p}_{h,1}$ is reserved for π^+ and $\vec{p}_{h,2}$ for π^-. This charge ordering is important; otherwise, the direction of $\vec{R}$ is randomized, resulting in a diluted asymmetry. The mechanism of producing azimuthal correlations and its extraction from a theoretical point of view can be found in Ref. [23].

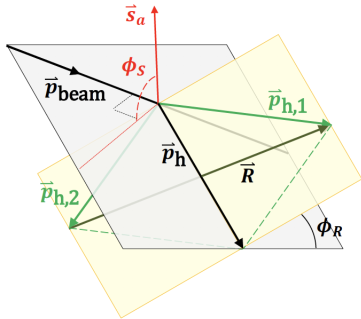

Figure 1: Azimuthal angles in the di-hadron system.

Particle tracks are selected by finding high-quality tracks associated with the event vertices within 60 cm along the beam direction from the nominal TPC center. Each track is required to have transverse momentum $p_T > 1.5$ GeV/c and the distance of closest approach dca < 1 cm from the event vertex. Charged pions are identified by measuring their ionization energy loss, dE/dx. Pions are selected by requiring a cut on the number of standard deviations of observed dE/dx (dE/dx_{obs}) from the expected pion energy loss ($dE/dx_{\pi,\text{calc}}$), $-1 < n\sigma_\pi < 2$, where $n\sigma_\pi = \frac{1}{\sigma_{\text{exp}}} \ln\left(\frac{dE/dx_{\text{obs}}}{dE/dx_{\pi,\text{calc}}}\right)$ with σ_{exp} being dE/dx resolution of the TPC.

The $\pi^+\pi^-$ pairs are formed by selecting oppositely charged pion tracks, and associated azimuthal angles ϕ_S and ϕ_R are constructed from di-pion kinematics as shown in Fig. 1. The π^+ and π^- tracks should be close enough in $\eta - \phi$ space (cone $\equiv \sqrt{(\eta^{\pi^+} - \eta^{\pi^-})^2 + (\phi^{\pi^+} - \phi^{\pi^-})^2} < 0.7$) to achieve a higher sensitivity to both pions originating from the same parton. The $\pi^+\pi^-$ yields are sorted based on the beam polarization direction ($\uparrow/\downarrow$) in 16 ϕ_{RS} bins. A_{UT} is then extracted from Eq. 1 as an amplitude of the sinusoidal fit over the range $[-\pi, 0]$. The analysis is performed for both polarized beams independently, considering the other as unpolarized. The final result is the weighted average of both.

3.2 Results

A_{UT} is measured as a function of $M_{inv}^{\pi^+\pi^-}$, $p_T^{\pi^+\pi^-}$, and $\eta^{\pi^+\pi^-}$. The $M_{inv}^{\pi^+\pi^-}$ dependence arises from the IFF, $p_T^{\pi^+\pi^-}$ sets the hard scale, and $\eta^{\pi^+\pi^-}$ is a surrogate for x, where higher x partons can be probed in the forward $\eta^{\pi^+\pi^-}$ region and vice-versa. Detailed results, including multi-dimensional binning, can be found in Ref. [34].

Figure 2 depicts A_{UT} as a function of $M_{inv}^{\pi^+\pi^-}$, integrated over $p_T^{\pi^+\pi^-}$, in the $\eta^{\pi^+\pi^-} > 0$ region, compared with the STAR 2006 result [15] and a theory curve (*gray band*) [35], which is fit to the SIDIS, e^+e^-, and STAR 2006 data. Both STAR measurements are in good agreement with the theory, showing a significant resonance peak at $M_{inv}^{\pi^+\pi^-} \sim M_\rho$, as expected in the IFF model calculation [23, 36].

Figure 3 shows A_{UT} as a function of $\eta^{\pi^+\pi^-}$, integrated over $M_{\text{inv}}^{\pi^+\pi^-}$ and $p_T^{\pi^+\pi^-}$ (*upper panel*). $\langle x \rangle$ and $\langle z \rangle$, the average fractional quark energy carried by the $\pi^+\pi^-$ pair, estimated from simulation, in the corresponding $\eta^{\pi^+\pi^-}$ bins are shown in the bottom panel. A_{UT} increases linearly with $\eta^{\pi^+\pi^-}$ in the forward $\eta^{\pi^+\pi^-}$ region, while the backward asymmetry signal is small, as expected. A strong correlation between the observed asymmetry and $\langle x \rangle$ can be seen, where $\langle x \rangle$ ranges from ~ 0.1 to 0.22 from backward to forward $\eta^{\pi^+\pi^-}$. However, $\langle z \rangle$ shows no clear dependence in $\eta^{\pi^+\pi^-}$, with an average of ~ 0.46.

The systematic uncertainty includes the effect of the bias in the event triggering (trigger bias) and particle identification (PID). The magnitude of the trigger bias is determined by calculating the fraction of quark events at the detector level (GEANT) and the particle level (PYTHIA) and taking a ratio between them. The size of the systematic effect related to the PID is estimated using

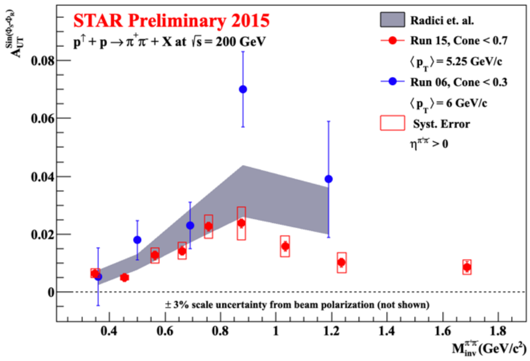

Figure 2: A_{UT} *vs.* $M_{inv}^{\pi^+\pi^-}$, in $\eta^{\pi^+\pi^-} > 0$ region, compared with the theoretical calculation from Ref. [35].

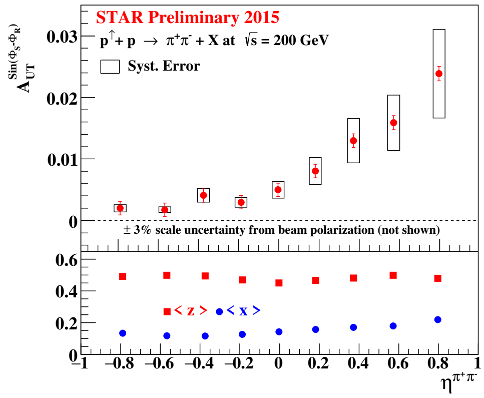

Figure 3: A_{UT} *vs.* $\eta^{\pi^+\pi^-}$, integrated over $M_{inv}^{\pi^+\pi^-}$ and $p_T^{\pi^+\pi^-}$ (*top panel*). The quark $\langle z \rangle$ and $\langle x \rangle$, in the corresponding $\eta^{\pi^+\pi^-}$ bins, are shown in the *bottom panel*.

$\pi^+\pi^-$ impurity ($\sim 20\% - 33\%$) in the respective asymmetry bins, which is the dominant systematic uncertainty at this stage of the analysis.

4. Unpolarized $\pi^+\pi^-$ Cross-Section

4.1 Event Selection, and Binning

All the event and track selection cuts and $\pi^+\pi^-$ construction procedure are similar to the one outlined in Sec. 3.1, except for the minimum track p_T cut, which is lowered to $p_T > 0.5$ GeV/c. Additionally, $\pi^+\pi^-$ events with cone falling below 0.02 are excluded. This minimum cone cut is intended to eliminate $\pi^+\pi^-$ events composed of tracks too close for separate identification by the detector. Furthermore, hard cuts are enforced on the pair p_T ($1 < p_T^{\pi^+\pi^-} < 15$ GeV/c) and pair mass ($0.27 < M_{inv}^{\pi^+\pi^-} < 4$ GeV/c^2) to further refine the $\pi^+\pi^-$ event selection.

The measurement of the differential unpolarized cross-section is performed in the $M_{inv}^{\pi^+\pi^-}$ bins. The minimum bin width is chosen based on a dedicated reconstruction performance study, and variable-width binning is considered to account for falling statistics with increasing mass. The total of thirteen bins are considered over the mass range of $0.27 < M_{inv}^{\pi^+\pi^-} < 4.0$ GeV/c^2. Unpolarized $\pi^+\pi^-$ cross-section is independently measured for JP0, JP1, and JP2 triggered events, and the final cross-section is the weighted average of all three triggered cross-sections.

4.2 Background Events

The potential sources of background are the beam backgrounds and pile-up events. The pions from the background events are identified by finding an association between the GEANT reconstructed and PYTHIA-generated true tracks. If any reconstructed pions in $\pi^+\pi^-$ are not associated with the truth level tracks, such pairs are considered backgrounds. Figure 4 (left panel) shows the data (red), background from simulation (blue), and background subtracted data (green) for the JP2 triggered events. The fraction of background is similar for the JP0 and JP1 triggered events as well. The background-subtracted data serves as an input for the unfolding.

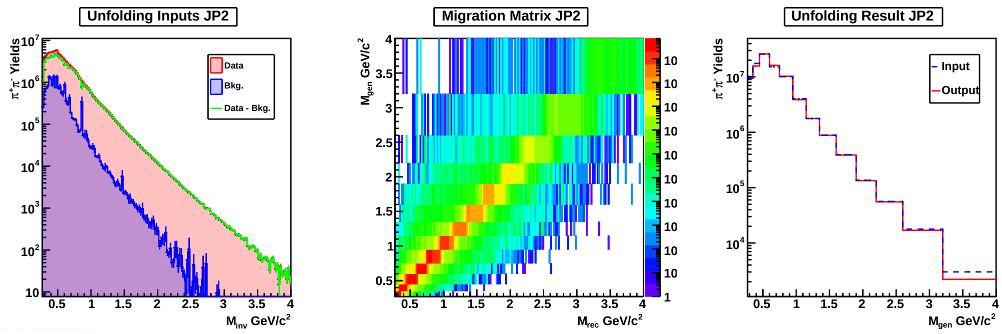

Figure 4: Left: Reconstructed $\pi^+\pi^-$ events (red), background events from simulation (blue), and background subtracted data (green). Middle: Migration matrix with true events along $y-$axis and reconstructed events along $x-$axis. Right: Input and unfolded distributions comparison for JP2 trigger.

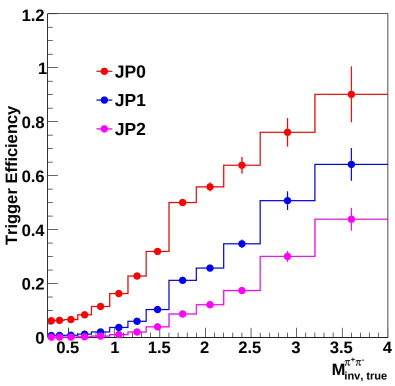

Figure 5: $\pi^+\pi^-$ triggering efficiency.

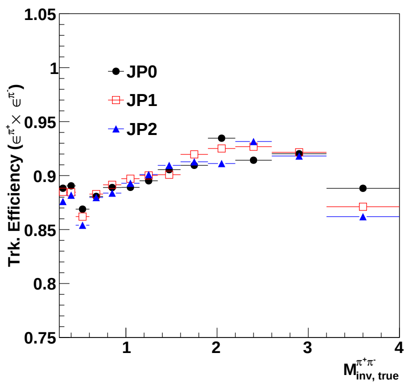

Figure 6: $\pi^+\pi^-$ tracking efficiency.

4.3 Unfolding

TUnfold algorithm [37] is used for the cross-section unfolding. The migration matrix, a two-dimensional matrix of $M_{inv}^{\pi^+\pi^-}$ with truth events along $y-$axis and reconstructed events along $x-$axis as shown in Fig. 4 (middle), was used as an input to the unfolding algorithm. Truth and reconstructed events in the migration matrix come from the PYTHIA and GEANT simulations, respectively. The input for the unfolding is a finely binned background subtracted yields (Fig. 4 (left panel)), and the unfolded output is in thirteen bins of variable width (truth bins). The unfolded distribution differs slightly from the input, with yields from the higher mass bins migrating to the lower mass region as shown in the right panel of Fig. 4. This final unfolded distribution is devoid of the bin migration effect and background. However, it still requires further corrections for the trigger and particle tracking efficiency to remove detector effects and corrections associated with the PID.

4.4 Corrections

All the corrections that are made to the unfolded cross-section are simulation-based. The correction factors are calculated in each cross-section bin for each trigger at the $\pi^+\pi^-$ level.

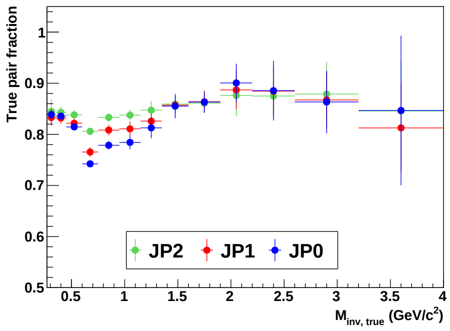

Figure 7: $\pi^+\pi^-$ purity fraction.

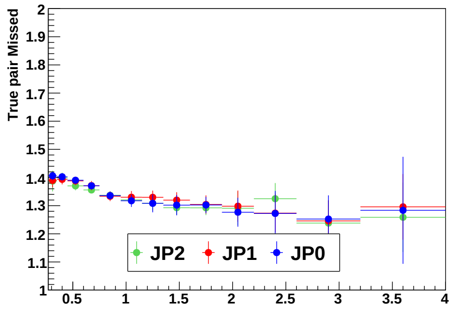

Figure 8: $\pi^+\pi^-$ loss fraction.

The trigger efficiency ($\epsilon_{trig}^{\pi^+\pi^-}$) is calculated as the fraction of triggered $\pi^+\pi^-$ events to the unbiased events, which have no knowledge of event triggering. The estimated values of $\epsilon_{trig}^{\pi^+\pi^-}$ for JP0, JP1, and JP2 triggered events are shown in Fig. 5, illustrating the trigger threshold conditions. The JP0 exhibits higher efficiency than the JP1 and JP2, which require successively higher threshold energy compared to JP0.

The pion tracking efficiency ($\epsilon_{trk}^{\pi^\pm}$) is estimated as the fraction of true tracks successfully reconstructed by the detector, whereas the tracking efficiency at the $\pi^+\pi^-$ level is a product of the π^+ and π^- tracking efficiencies. Figure 6 illustrates the $\epsilon_{trk}^{\pi^+\pi^-}$ as a function of $M_{inv}^{\pi^+\pi^-}$ for JP0, JP1, and JP2 triggered events, which consistently exceeds 85% throughout the $M_{inv}^{\pi^+\pi^-}$ range. $\epsilon_{trk}^{\pi^+\pi^-}$ shows slight mass dependence; however, there is no significant trigger dependence.

At the data level, pions are selected based on a dE/dx cut, which non-pion backgrounds may contaminate. The purity of $\pi^+\pi^-$ (f_{true}) for the cross-section correction is estimated as the fraction of true $\pi^+\pi^-$ events that fall within the default $\pi^+\pi^-$ selection cut $-1 < n\sigma_\pi < 2$ cut. Fig. 7 shows the f_{true} in cross-section bins for all three JP triggers. f_{true} exhibits a slight mass dependence, increasing as the mass increases. Additionally, the fraction has a trigger dependence, specifically around the $\rho-$mass region.

Some of the true $\pi^+\pi^-$ may be lost due to the restrictive PID cut, consequently lowering the cross-section. The fraction of lost true $\pi^+\pi^-$ (f_{loss}), shown in Figure 8, that falls outside the PID cut accounts for the inefficiency of the applied PID cut in identifying pion. This fraction is greater than one and increases the yields by this factor to account for the loss of $\pi^+\pi^-$ events. The f_{loss} is independent of the triggers, varying from 1.4 at the lower mass region to 1.3 at the higher mass regions.

4.5 Result

With all the components on hand, the cross-section per trigger can be calculated as $\frac{d\sigma_{UU}^{\pi^+\pi^-}}{dM} = \frac{f_{true} \cdot f_{loss}}{\mathcal{L} \cdot \epsilon_{trk}^{\pi^+\pi^-} \cdot \epsilon_{trig}^{\pi^+\pi^-}} \cdot \frac{dN^{\pi^+\pi^-}}{dM}$, where $\frac{dN^{\pi^+\pi^-}}{dM}$ is the unfolded yield normalized by the bin width and $\mathcal{L}$ is the luminosity per trigger. The calculated luminosity values are 0.16, 7.68, and 18.80 pb^{-1} for JP0, JP1, and JP2 trigger, respectively. The measured cross-section is a weighted average of JP0, JP1, and JP2 triggered cross-sections, depicted in red in the top panel of Fig. 9. The total systematic uncertainty, shown as a green-hatched band, is presented alongside the data points. The

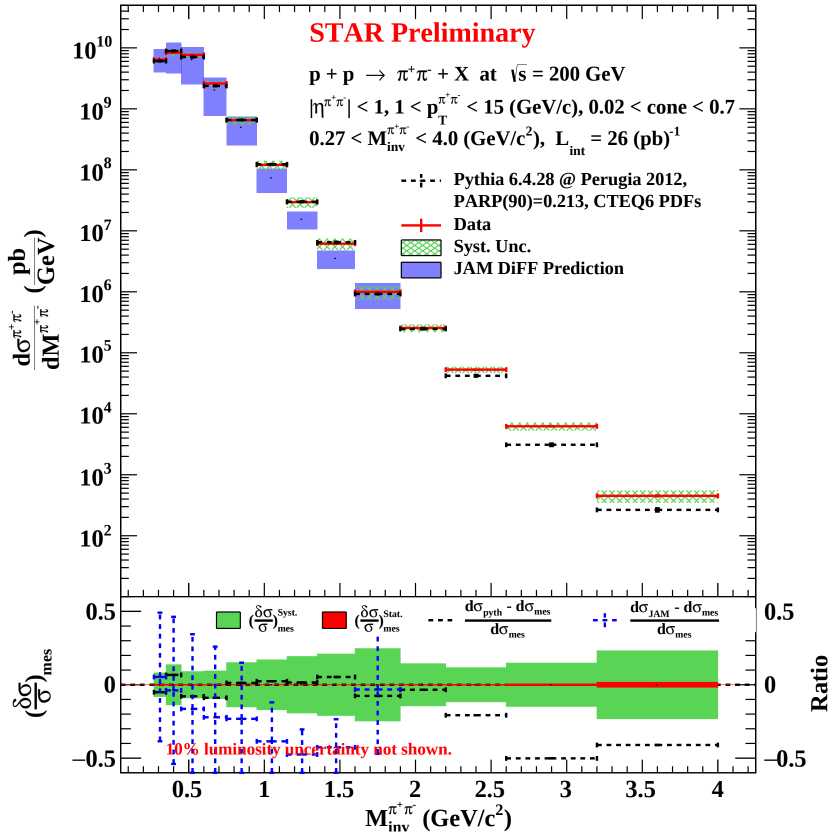

Figure 9: Unpolarized $\pi^+\pi^-$ cross-section compared with the PYTHIA and JAM cross-sections.

absolute PYTHIA (version and tune details as described in Sec. 2) cross-section is represented by a dashed black line and theoretical prediction from the JAM collaboration is depicted in purple band [6, 38]. The uncertainty band in the JAM cross-section is purely statistical, arising from taking the mean and average of ($\sim$ 300) replicas. The agreement between the measured cross-section, PYTHIA, and theoretical predictions is excellent and falls within the uncertainty bounds. This consistency demonstrates the reliability of the analysis framework and its alignment with theoretical expectations. Notably, the measured cross-section encompasses $\pi^+\pi^-$ production from quark and gluon fragmentation. Consequently, this marks a significant step toward constraining the gluon fragmentation function, a leading source of uncertainty in the transversity.

In the bottom panel, the green band represents the total systematic uncertainty comprising various effects associated with the PID and efficiencies, which is dominated by the effect related to the trigger efficiencies. The red band indicates the statistical uncertainty. Closed black circles depict the relative difference between the PYTHIA and measured cross-sections, and the dashed blue lines illustrate the relative difference between the JAM DiFF prediction and the final cross-section. The 10% uncertainty from the luminosity measurement is not included in the final uncertainty.

5. Summary and Outlook

STAR has measured $\pi^+\pi^-$ correlation asymmetries based on 2015 $p^\uparrow p$ data and the first unpolarized $\pi^+\pi^-$ cross-section using 2012 data at $\sqrt{s}$ = 200 GeV. These datasets cover Q^2 at the order of $\sim$ 100 GeV^2 at intermediate x ($0.1 < x < 0.3$), where the transversity is expected to be sizable.

The measured IFF asymmetry signal is enhanced around $M_{inv}^{\pi^+\pi^-} \sim 0.8$ GeV/c^2, which is consistent with the theoretical calculation and the previous STAR measurements. A large asymmetry in the forward $\eta^{\pi^+\pi^-}$ region corresponds to higher x, where quark transversity is expected to be sizable. In contrast, the backward asymmetries are small since they probe polarized low-x quarks and scattered quarks from the unpolarized beam. The statistical precision of these results is largely improved compared to the previous STAR results. The systematic uncertainty includes the effect of the PID and trigger bias. The large systematic uncertainty is dominated by the PID, which is better understood and expected to reduce significantly, including the TOF PID.

The unpolarized $\pi^+\pi^-$ cross-section differential in $M_{inv}^{\pi^+\pi^-}$ in a proton-proton collision at $\sqrt{s}$ = 200 GeV has been measured for the first time using STAR Run 2012 data. The measured cross-section shows good agreement with the PYTHIA cross-section and the theoretical prediction from the JAM collaboration. This unpolarized cross-section result in pp is much needed to constrain the gluon fragmentation function and, consequently, transversity.

These high-precision IFF asymmetries, combined with the unpolarized cross-section result from STAR in pp collisions, complement SIDIS and e^+e^- data, providing a foundation for a model-independent extraction of transversity with greater precision than previously possible.

References

[1] H. Abramowicz *et al.*, Eur. Phys. J. C **75**(12), 580 (2015)

[2] D. de Florian, R. Sassot, M. Stratmann and W. Vogelsang, Phys. Rev. D **80**, 034030 (2009)

[3] M. Anselmino *et al.*, Phys. Rev. D **87**, 094019 (2013)

[4] Z. B. Kang, A. Prokudin, P. Sun and F. Yuan, Phys. Rev. D **93**, no.1, 014009 (2016)

[5] M. Radici and A. Bacchetta, Phys. Rev. Lett. **120**, no.19, 192001 (2018)

[6] C. Cocuzza *et al.*, [arXiv:2308.14857 [hep-ph]]

[7] A. Airapetian *et al.* [HERMES], JHEP **06**, 017 (2008)

[8] A. Airapetian *et al.* [HERMES], Phys. Rev. Lett. **103**, 152002 (2009)

[9] M. Alekseev *et al.* [COMPASS], Phys. Lett. B **673**, 127-135 (2009)

[10] C. Adolph *et al.* [COMPASS], Phys. Lett. B **713**, 10-16 (2012)

[11] C. Adolph *et al.* [COMPASS], Phys. Lett. B **744**, 250-259 (2015)

[12] X. Qian *et al.* [Jefferson Lab Hall A], Phys. Rev. Lett. **107**, 072003 (2011)

[13] J. P. Lees *et al.* [BaBar], Pys. Rev. D **90**, no.5, 052003 (2014)

[14] R. Seidl *et al.* [Belle], Phys. Rev. D **78**, 032011 (2008) [erratum: Phys. Rev. D **86**, 039905 (2012)]

[15] L. Adamczyk *et al*. [STAR Collaboration], Phys. Rev. Lett. **115**, 242501 (2015)

[16] L. Adamczyk *et al*. [STAR Collaboration], Phys. Lett. B **780**, 332 (2018)

[17] J. C. Collins, Nucl. Phys. B **396** (1993), 161-182

[18] U. D'Alesio, C. Flore and A. Prokudin, Phys. Lett. B **803** (2020), 135347

[19] J. Cammarota *et al.* [Jefferson Lab Angular Momentum], Phys. Rev. D **102** (2020) no.5, 054002

[20] J. Tang, [arXiv:hep-ph/9807560 [hep-ph]].

[21] R. L. Jaffe, X. m. Jin and J. Tang, Phys. Rev. Lett. **80** (1998), 1166-1169

[22] R. L. Jaffe, X. m. Jin and J. a. Tang, Phys. Rev. D **57** (1998), 5920-5922

[23] Bacchetta *et al*., Phys. Rev. D **70**(9) (2004)

[24] K. H. Ackermann *et al.* [STAR], Nucl. Instrum. Meth. A **499** (2003), 624-632

[25] M. Anderson *et al.* Nucl. Instrum. Meth. A **499** (2003), 659-678

[26] W. Llope, Nucl. Instrum. Meth. **241**(1), 306 (2005)

[27] M. Beddo *et al.* [STAR], Nucl. Instrum. Meth. A **499** (2003), 725-739

[28] T. Sjostrand, S. Mrenna and P. Z. Skands, JHEP **05** (2006), 026

[29] P. Z. Skands, Phys. Rev. D **82** (2010), 074018

[30] J. K. Adkins, [arXiv:1907.11233 [hep-ex]]

[31] J. Pumplin *et al.*, JHEP **07** (2002), 012

[32] R. Brun *et al*., CERN, Geneva (1978).

[33] G. G. Ohlsen and P. Keaton, Nucl. Instrum. Meth. **109**(1), 41 (1973)

[34] B. Pokhrel, JPS Conf. Proc. **37** (2022), 020121

[35] M. Radici, Private communication

[36] A. Bacchetta and M. Radici, Phys. Rev. D **67**, 094002 (2003)

[37] S. Schmitt, JINST **7** (2012), T10003

[38] C. Cocuzza, Private communication